**ICMIEE20-046**

# Finite Element Simulation of Flow Stress and Its Implications for Machining Process Optimization

*Dibakar Sarker*[*]*, Khalid Bin Mosharof, Shams Abu Alam, M. Azizur Rahman*
Department of Mechanical & Production Engineering, Ahsanullah University of Science and Technology, Dhaka-1208, BANGLADESH

**ABSTRACT**
In metallic ultra-precision machining, the flow stress model has a significant influence in determining the ploughing effect from the manifestation of chip separation. The distinction of material deformation (in ploughing) and lamella formation (in chip separation) is realized by the relative tool sharpness (RTS), which is obtained by dividing the thickness of undeformed chip with cutter edge radius. The study discussed here demonstrates the 'flow stress phenomenon' with the help of finite element (FE) simulation in metal cutting operation using Simulia Abaqus Computer-Aided Engineering (CAE) software. The model is developed in orthogonal turning process of aluminum alloy workpiece for the occurrence of continuous and discontinuous chips. The Johnson-Cook damage model was used for workpiece deformation and input boundary conditions (BC) in Abaqus CAE were provided for creating a simulation intended to compare the FE data with experimented results. The simulated results showed consistency with experimental results in certain criteria which have been explained with proper justifications. The implications of this study lie in the flow stress model verified through simulation and further opportunity for optimization and improvement.

Keywords: Machining, Flow stress, FE Simulation, Abaqus CAE, Optimization

## 1. Introduction

Ultra-precision machining (UPM) refers to a set of non-conventional atomic scale manufacturing processes where single crystal diamond (SCD) tools are deployed to achieve ultra-fine surface in the locality of 1 nm [1]. UPM is applied using high specific energy in producing numerous high-precision mechanical, electronic and optical 3D complex parts where surface quality is a primary consideration for nano-level finishing. For UPM to be suitable for making micro-products, analysis of single or multi-crystal material behavior with tool-workpiece interface guiding the operational forces is of paramount importance [2], unlike conventional machining [3]. Consequently, multiscale FE modeling of different UPM processes for deeper understanding of cutting mechanisms has become a point of interest for researchers [4].

Numerous factors act behind the nanometric surface quality produced in UPM such as machine tool, cutting and environment conditions, tool geometry, vibration, tool wear, chip formation mechanics, tool rake angle, and material properties where understanding the physics of material separation remains crucial [5]. To measure the effects of cutting edge geometry along with microstructural tool-work interaction, a term called relative tool sharpness (RTS) defined to be the ratio of undeformed chip thickness ($h_c$) to tool edge radius ($r_n$) [6]. Different alloys show different behaviors on specific cutting energy and cutting forces when RTS is varied [7].

For cutting processes to deliver dimensional accuracy, a growing set of soft computing techniques and algorithms are being used [8]. All these methods are applied to minimize defects, reduce the number of trial and error, and improve product value through predictions [9]. With the rise of Industry 4.0 and smart manufacturing [10], many decision-making processes by human operator are being replaced by preexisting databases which is leading to the novel field of intelligent machining with better control over the overall machining sequence than conventional methods [11].

FE modeling is broadly used in machining as a means of numerical simulation technique where large deformations occur in comparatively small regions of chip separation and it can decrease the cost and hassle of prototyping [12]. Among several commercial FE software, the Abaqus CAE (Complete Abaqus Environment) comes with a set of tools for preprocessing mechanical models and assemblies and visualizing FE analysis results. It is generally capable of modeling failure and progressive damage of ductile materials in association with the Johnson-Cook (JC), the Mises, Hill, and Drucker-Prager plasticity models [13].

This paper builds up on this theory by simulating chip formation using Abaqus CAE version 6.14.2. The JC plasticity model has been utilized in the interface to get simulated results. Additionally, the usefulness of scalable intelligent machining approach on this topic has been discussed.

## 2. Technical Background

In UPM, the chip formation technique heavily influences the quality of the produced surface. The theories used in this study has been discussed in section 2.1-2.2.

### 2.1 Influence of RTS in UPM

RTS values dictates the material removal mechanism type by four distinguished independent surface generation behaviors: shearing, extrusion, ploughing and rubbing [14]. RTS has evolved from the concept called "cutting edge radius" in machining where $r_n$ is larger than $h_c$. which showed that material beside the

* Corresponding author. Tel.: +88-01521333330
E-mail addresses: dibakarsarker89@gmail.com

tool edge creates two types of flows: chip flowing above the rake face and the other flow compressed underneath the face of the tool's flank shown in Fig.1 (a) [15]. Also, plastic deformation by compressive stress in front of the cutting edge is caused by ploughing effect as depicted in Fig.1 (b).

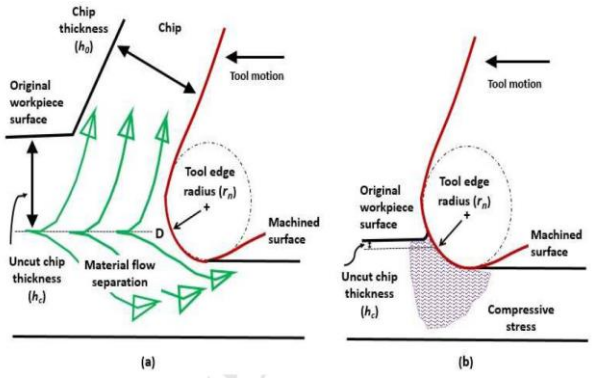


**Fig.1** Diagram showing (a) effect of cutting (separation) at RTS >> 1.0 [16] (b) effect of ploughing (rake angle is negative) at RTS << 1.0 [17]

To get desired surface quality in UPM, it is essential to discriminate flow separation of material (cutting) from deformation of material (rubbing and ploughing) as shown in Fig.2.

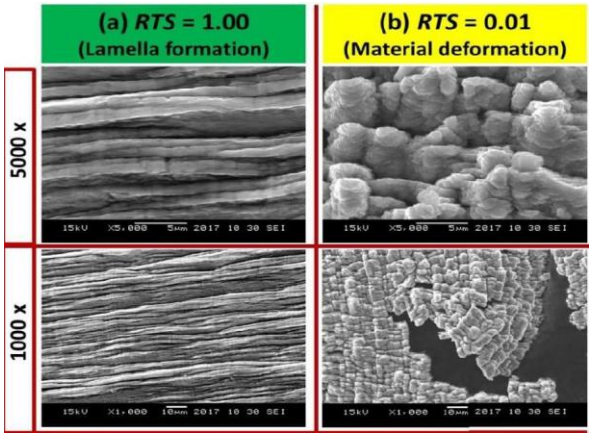


**Fig.2** Magnified SEM Pictures of Al6082 (a) lamella formation at RTS = 1.00 and (b) deformed material at RTS = 0.01 [15]

2.2 The Johnson-Cook (JC) Damage Model and Overall Material Flow Stress

The JC damage model (1985) is heavily used in FE analysis of high strain rate plastic deformation of most metals due to its mathematical straightforwardness and capability to predict metal working situations of first-order [18]. The JC plasticity model acts as a representation of cumulative damage as follows [19]:

*Strength Model:* Mises tensile flow stress,

$$\sigma = ( A + B \varepsilon^{n} ) ( 1 + C \ln\dot{\varepsilon}^{*} ) ( 1 - T^{*m} ) \text{ ----------(1)}$$

*Fracture Model:* Fracture strain depending on triaxiality ratio, temperature and strain rate is given by,

$$\varepsilon^{f} = [ D_1 + D_2 \exp D_3 \sigma^{*}] [1 + D_4 \ln\dot{\varepsilon}^{*} ] [ 1 + D_5 T^{*} ] \text{ ---(2)}$$

where $D_1$ to $D_5$ are damage model constants, $T^{*}$ is identical to $T^{*m}$ in Equation (1) and the pressure stress ratio, $\sigma^{*} = \sigma_m / \bar{\sigma}$

The damage to an element, $D = \sum (\Delta\varepsilon/\varepsilon^{f})$ ----------(3)

The overall material flow stress for a material in UPM as a summation of flow stress of surface layer and flow stress of gliding dislocations is given by [15]:

$$\sigma = (M\tau_R + \frac{k_{HP}}{\sqrt{d}}) - (\frac{d}{h_n}) (M\tau_R + \frac{k_{HP}}{\sqrt{d}} - m\tau_R) + M\alpha_d G\sqrt{\frac{bk_b\theta_{av}}{d}} \text{ ----------(4)}$$

which is tantamount to the Mises flow stress in Equation (1) connecting crystallographic effects of chip development with chip thickness ($h_o$) and grain size (d).

## 3. Finite Element (FE) Simulation of Machining Using Abaqus CAE

The Abaqus CAE possess a dedicated input module for JC damage parameters as shown in Fig.3.

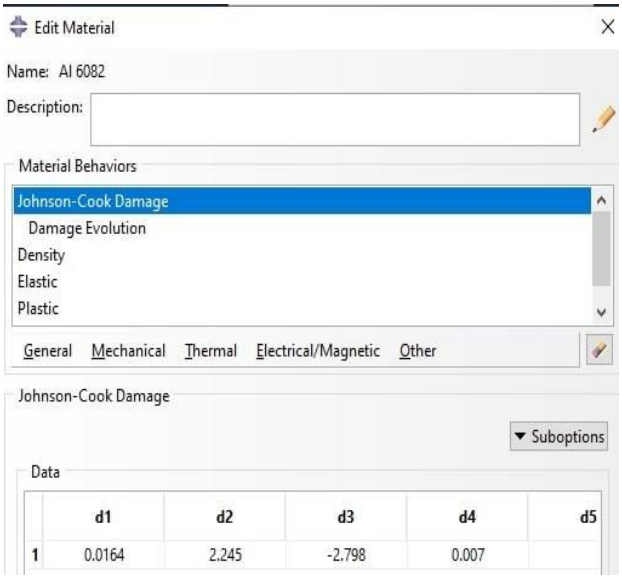


**Fig.3** JC damage module for materials in Abaqus CAE

To demonstrate the differences between conventional machining and UPM, first of all, two simulations were performed using a conventional sharp tool model without considering tool edge radius ($r_n$) that produced discontinuous and continuous chips as shown in Fig. 4 & 5 respectively with their von Mises stresses. The global element sizes were set to 0.002 mm for workpiece and 0.0005 mm for cutter with the purpose of displaying chip formation only.

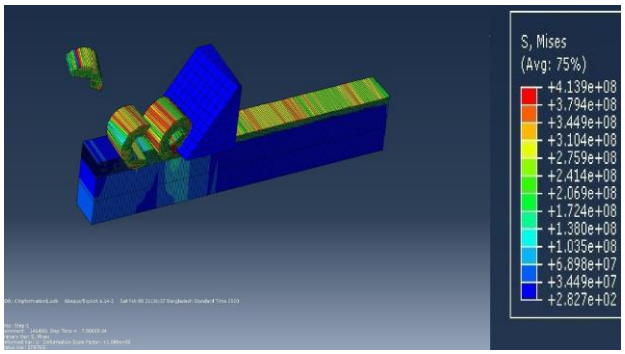


**Fig.4** Conventional segregated chip formation in Abaqus CAE interface

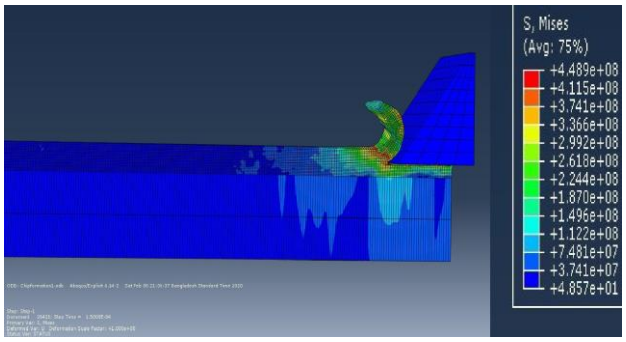


**Fig.5** Conventional continuous chip formation in Abaqus CAE

Then, $r_n$ = 15.5 µm (0.0155 mm) was considered in simulation like the physical experiment [15] for testing the effects of edge radius and RTS. Using the data mentioned in Table 1 & 2, a series of FE simulations of the aforementioned orthogonal ultra-precision turning process was performed in Abaqus CAE that demonstrated the mechanical process of UPM. The thermal implications were ignored because of simplicity and lower heat generation in the workpiece compared to the tool in UPM [20] and the cutting tool was considered as a hard rigid body without damage.

**Table 1** Modified JC material constraints used in simulation for Al6082-T6 workpiece [21]

| Material Property | Value |
|---|---|
| Yield stress, A [MPa] | 403.57 |
| Strain hardening, B [MPa] | 306.56 |
| Strain hardening index, n | 0.7769 |
| Initial failure strain, d1 ($D_1$) | 0.0164 |
| Exponential factor, d2 ($D_2$) | 2.245 |
| Triaxiality factor, d3 ($D_3$) | -2.798 |
| Strain rate factor, d4 ($D_4$) | 0.007 |

**Table 2** Physical properties of Al6082-T2

| Property | Value | Unit |
|---|---|---|
| Young's modulus | 70 | GPa |
| Poisson's ratio | 0.33 | - |
| Density | 2700 | Kg/m$^3$ |

Other conditions for input:

- Mesh Sensitivity Criteria:
  Two global mesh sizes for RTS=1.0 and RTS = 0.06 have been used for mesh sensitivity analysis in Fig.6-9 which has been discussed in section 4.
  *1st Criterion:* Global Seed Size = 0.001 Mesh Size (lengthwise/x-axis) = 0.00033 Mesh Size (height/y-axis) = 0.00052
  *2nd Criterion:* Global Seed Size = 0.00025 Mesh Size (lengthwise/x-axis) = 0.0002 Mesh Size (height/y-axis) = 0.00031
  Here, all dimensions are calculated and applied to be expressed in millimeters (mm) as Abaqus CAE does not inherently possess options for units.
- Boundary Conditions (BC) [22]:
  Here, U1 & U2 depict translational movement of bodies along x- & y-axis respectively. UR1 & UR2 represent rotations centering x- & y-axis respectively.
  For cutter, initially U1 = 0 since no cutting process exists in the beginning. After the process initiation, U1 = -0.1, U2 = 0, UR1=UR2 =0
  For workpiece, "encastre" option was used as BC so it remains still without any movement along any direction. Therefore, U1=U2=UR1=UR2=0

The simulated phenomena are depicted in Fig.6-9 with the von Mises stress values indicated on the left.

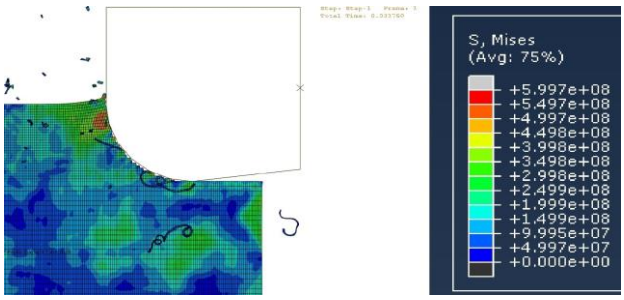


**Fig.6** 1st criterion chip formation for RTS = 1

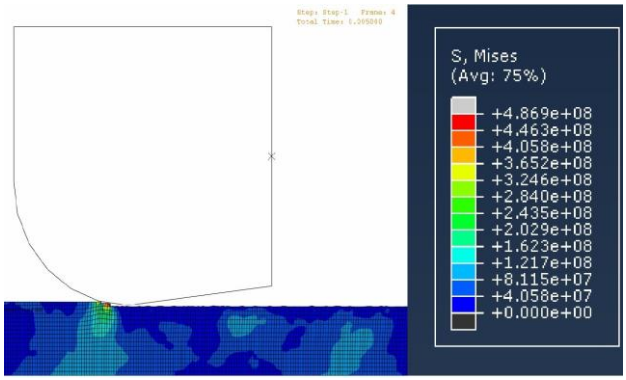


**Fig.7** 1st criterion chip formation for RTS = 0.06

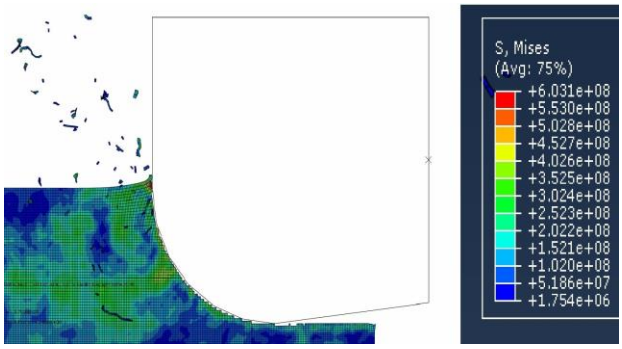


**Fig.8** 2nd criterion chip formation for RTS = 1

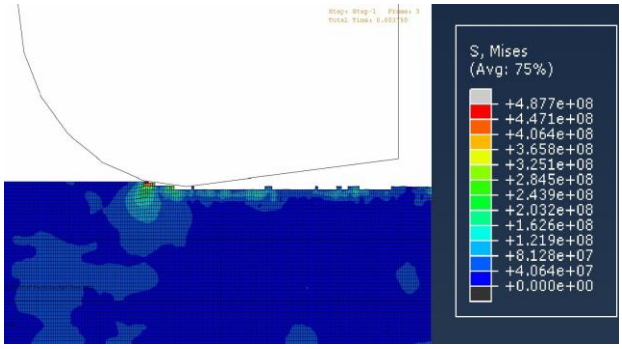


**Fig.9** 2nd criterion chip formation for RTS = 0.06

## 4. Comparison with Experimental Results

Experimental results [15] showed that at higher RTS values cause lamella formation in chips while lower RTS values cause material deformation. At higher RTS values chips become larger than at lower RTS values.

When the simulation process was attempted in Abaqus CAE with RTS = 0.01, no chip formation could be observed just like the experimental results [15] which required scanning electron microscopy (SEM) for visibility. The simulation was tested with RTS = 1 and RTS = 0.06 afterwards for comparison with experimental results using two criteria (mesh sizes) discussed in section 3 for gauging the proper element sizes. The comparisons for both criteria are given in Table 3 & 4.

**Table 3** Comparison for 1st criterion of meshing

| Fig. No. | RTS | Chip Type | Machined Surface Type | Consistency with Experiment |
|---|---|---|---|---|
| 6 | 1 | Continuous with breakage | No cracks | Fairly consistent chips & surface |
| 7 | 0.06 | Barely visible | Coarse | Slightly consistent surface (for grain size 216.8 µm) |

**Table 4** Comparison for 2nd criterion of meshing

| Fig. No. | RTS | Chip Type | Machined Surface Type | Consistency with Experiment |
|---|---|---|---|---|
| 8 | 1 | Incomplete | Coarse | Inconsistent chips & surface |
| 9 | 0.06 | Barely visible | Visibly cracked | Consistent surface (for grain size 216.8 µm) |

From Table 3 & 4 it is clear that the 1st criterion of meshing (global element size = 0.001 mm, Fig. 6) for RTS = 1 and 2nd criterion of meshing (global element size = 0.00025, Fig. 9) for RTS = 0.06 expressed the greatest consistency with the experimental results in terms of qualitative visual assessment of the machining experiment and the simulation outputs. Therefore, these element sizes showed better sensitivity in simulation.

The FE simulations in Fig.4-9 also display von Mises yield stresses occurring in the operations which reveals the maximum stress concentrated in every shear plane where the primary deformation zone of finite thickness and width was located which conforms to practical orthogonal cutting model [23]. The element sizes were taken considering the limit of processing power of the hardware. Given superior computer processing power and more simulation time, the accuracy of simulated results can be increased as simulated chip geometry would then conform to the experimental characteristics to a higher degree [12]. Also, availability of dedicated conditions for several grain sizes of material in simulation tool would certainly improve results.

## 5. Conclusion

In this study, a simulated chip formation of a UPM turning operation based on the JC damage model was performed in Abaqus CAE using a set of selected variables of the Mises flow stress equation that showed several consistencies with previous experiments, including generated surface types and chip characteristics. The following conclusions can be noted from the study performed: -

- The variation of RTS in experimental and simulated environments plays the central role in determining the nature of chip and surface.
- The flow stress model can be justified using simulated results which agrees with physical experimentation.
- The generated surface type is the most substantial aspect in UPM due to its intrinsic characteristics that demand intelligent process optimization methods.
- The simulated results can be improved by software interfaces that allows for grain size and higher processing power.

The significance of intelligent machining and simulated testing of machined surface generation like

this study dominate within the range of Industry 4.0 which calls for extensive research as a cost-effective means of predicting surface properties. Further elaboration on the current study and extension on the applications of algorithmic optimization methods and experimentation will appear in upcoming works.

## 6. References


[1] S. S. Joshi, "Ultraprecision Machining (UPM)," in *Encyclopedia of Nanotechnology*, B. Bhushan, Ed. Springer Reference, 2016.

[2] S. To, W. B. Lee, and C. Y. Chan, "Ultraprecision diamond turning of aluminium single crystals," *J. Mater. Process. Technol.*, vol. 63, no. 1–3, pp. 157–162, Jan. 1997.

[3] D. Dornfeld and D. E. Lee, *Precision manufacturing*. Boston, MA: Springer US, 2008.

[4] X. Luo, K. Cheng, D. Webb, and F. Wardle, "Design of ultraprecision machine tools with applications to manufacture of miniature and micro components," *J. Mater. Process. Technol.*, vol. 167, no. 2–3, pp. 515–528, 2005.

[5] S. J. Zhang, S. To, S. J. Wang, and Z. W. Zhu, "A review of surface roughness generation in ultra-precision machining," *Int. J. Mach. Tools Manuf.*, vol. 91, pp. 76–95, 2015.

[6] J. C. Outeiro and V. P. Astakhov, "The role of the relative tool sharpness in modelling of the cutting process," in *Proceedings of the 8th CIRP International Workshop on Modelling of Machining Operations*, 2005, pp. 517–524.

[7] M. A. Rahman, K. S. Woon, V. C. Venkatesh, and M. Rahman, "Modelling of the combined microstructural and cutting edge effects in ultraprecision machining," *CIRP Ann.*, vol. 67, no. 1, pp. 129–132, 2018.

[8] M. Chandrasekaran, M. Muralidhar, C. M. Krishna, and U. S. Dixit, "Application of soft computing techniques in machining performance prediction and optimization: A literature review," *Int. J. Adv. Manuf. Technol.*, vol. 46, no. 5–8, pp. 445–464, Jan. 2010.

[9] S. Chakraborty, B. Bhattacharyya, and S. Diyaley, "Applications of optimization techniques for parametric analysis of non-traditional machining processes: A review," *Manag. Sci. Lett.*, vol. 9, no. 3, pp. 467–494, 2019.

[10] R. Y. Zhong, X. Xu, E. Klotz, and S. T. Newman, "Intelligent Manufacturing in the Context of Industry 4.0: A Review," *Engineering*, vol. 3, no. 5, pp. 616–630, Oct. 2017.

[11] M. Chen, C. Wang, Q. An, and W. Ming, "Tool path strategy and cutting process monitoring in intelligent machining," *Front. Mech. Eng.*, vol. 13, no. 2, pp. 232–242, 2018.

[12] C. H. Lauro, L. C. Brandão, S. L. M. R. Filho, R. A. F. Valente, and J. P. Davim, "Finite Element Method in Machining Processes: A Review," in *Modern Manufacturing Engineering*, J. P. Davim, Ed. Springer, Cham, 2015, pp. 65–97.

[13] "About progressive damage and failure." [Online]. Available: https://abaqus-docs.mit.edu/2017/English/SIMACAEMATRefMap/simamat-c-damageoverview.htm#simamat-c-damageoverview. [Accessed: 01-Jul-2020].

[14] M. A. Rahman, M. R. Amrun, M. Rahman, and A. S. Kumar, "Variation of surface generation mechanisms in ultra-precision machining due to relative tool sharpness (RTS) and material properties," *Int. J. Mach. Tools Manuf.*, vol. 115, pp. 15–28, 2017.

[15] M. A. Rahman, M. Rahman, and A. S. Kumar, "Modelling of flow stress by correlating the material grain size and chip thickness in ultra-precision machining," *Int. J. Mach. Tools Manuf.*, vol. 123, pp. 57–75, 2017.

[16] C. Rubenstein, W. S. Lau, and P. K. Venuvinod, "Flow of workpiece material in the vicinity of the cutting edge," *Int. J. Mach. Tool Des. Res.*, vol. 25, no. 1, pp. 91–97, Jan. 1985.

[17] F. Z. Fang, H. Wu, and Y. C. Liu, "Modelling and experimental investigation on nanometric cutting of monocrystalline silicon," *Int. J. Mach. Tools Manuf.*, vol. 45, no. 15, pp. 1681–1686, 2005.

[18] M. Grujicic, B. Pandurangan, C. F. Yen, and B. A. Cheeseman, "Modifications in the AA5083 Johnson-Cook material model for use in friction stir welding computational analyses," *J. Mater. Eng. Perform.*, vol. 21, no. 11, pp. 2207–2217, Nov. 2012.

[19] G. R. Johnson and W. H. Cook, "Fracture characteristics of three metals subjected to various strains, strain rates, temperatures and pressures," *Eng. Fract. Mech.*, vol. 21, no. 1, pp. 31–48, 1985.

[20] T. Moriwaki, A. Horiuchi, and K. Okuda, "Effect of Cutting Heat on Machining Accuracy in Ultra-Precision Diamond Turning," *CIRP Ann. - Manuf. Technol.*, vol. 39, no. 1, pp. 81–84, 1990.

[21] W. Sawangsri and K. Cheng, "Investigation on partitioned distribution of cutting heat and cutting temperature in micro cutting," *Int. J. Mechatronics Manuf. Syst.*, vol. 9, no. 2, pp. 173–195, 2016.

[22] "Defining a base motion boundary condition." [Online]. Available: https://abaqus-docs.mit.edu/2017/English/SIMACAECAERefMap/simacae-t-lbibceditorsbasemotion.htm. [Accessed: 27-Jun-2020].

[23] S. Lee, J. Hwang, M. Ravi Shankar, S. Chandrasekar, and W. D. Compton, "Large strain deformation field in machining," *Metall. Mater. Trans. A Phys. Metall. Mater. Sci.*, vol. 37, no. 5, pp. 1633–1643, May 2006.

**NOMENCLATURE**

A : Yield stress, MPa
B : Strain hardening, MPa
M : Taylor factor
$d$ : Grain size, μm
$\sigma_m$ : Average of three normal stresses, MPa
$\bar{\sigma}$ : von Mises equivalent stress, MPa
$\alpha_d$ : Material constant
$b$ : Burgers vector, nm
G : Shear modulus, GPa
$m$ : Schmid factor
$k_b$ : Geometry boundary constant
$\tau_R$ : Shear stress, MPa
$\theta_{av}$ : Average misorientation angle, deg
$k_{HP}$ : Hall-Petch coefficient, MPa√μm
ε : Equivalent plastic strain
$\dot{\varepsilon}^*$ : Dimensionless plastic strain rate
Δε : Equivalent plastic strain increment
$T^{*m}$ : Homologous temperature, K
$h_o$ : Chip thickness, mm
$r_n$ : Tool edge radius, mm